Pore-Space Dynamics in a Soil Aggregate Bed under a Static External Load

Teamrat A. Ghezzehei* and Dani Or

ABSTRACT

The loose and fragmented soil structure that results from tillage operations provides favorable physical conditions for plant growth. This desirable state is structurally unstable and deteriorates with time because of overburden, external stresses, and capillary forces. The objective of this study was to model these structural changes by coupling soil intrinsic rheological properties with geometry and arrangement of aggregates represented as monosized spheres. Calculations of interaggregate stresses and strains, and associated changes in density and porosity, were performed for a rhombohedral unit cell. Soil rheological properties determined by application of steady shear stress were used for calculations of strains under steady interaggregate stresses. The models developed herein correspond to the initial stage of deformation when discrete aggregates exist. At strains exceeding 0.12 the interaggregate voids are isolated and the current model no longer applies and an alternative approach is presented elsewhere. Unit cell calculations were up scaled to an aggregate-bed scale by considering a one-dimensional stack of unit cells, which allows only vertical stress transmission. The stress acting at an interaggregate contact is fully accommodated (dissipated) by viscous flow when it exceeds the yield stress (strength) of the aggregates. The stress is fully transmitted to subsequent unit cells when it is less than the yield stress. Plausibility of the models was demonstrated by illustrative examples that highlight the different features of the models. The results were in qualitative agreement with observations from the literature for deformation of either loose structure, and for highly dense cases close to maximal bulk density.

Tillage of agricultural soil results in a loose and fragmented structure where aggregates are separated from each other by interaggregate voids. The total volume and size distribution of these voids determine important soil physical characteristics, such as air and water conductivities, water retention, and mechanical resistance to plant root growth. This loose structure settles because of compaction by farm implements and surface tension of pore water, and consolidation by overburden (Koolen and Kuipers, 1989).

Settlement and increase in strength of agricultural soils because of various factors are often quantified using bulk empirical stress–strain relationships such as the Mohr–Coulomb curves (e.g., Horn et al., 1998; Kirby, 1994; Kirby et al., 1997; Koolen and Kuipers, 1989; Lebert et al., 1989). Often, the soil mechanical coefficients used in these constitutive relationships have no clear physical meaning (Oda and Iwashita, 1999). Moreover, bulk settlement and strength changes alone are not sufficient to describe evolution of soil hydraulic properties. Recently, we proposed alternative framework for modeling evolution of soil structure by focusing on individual soil aggregates and interaggregate pores (Ghezzehei and Or, 2000; Ghezzehei and Or, 2001; Or, 1996). This framework considers spherical soil aggregates and interplay between soil rheology, capillary forces, and external stresses. We used stochastic formulation to upscale the single-pore dynamics to evolution of sample scale pore-size distribution (Or et al., 2000).

The objective of this study is to extend the earlier framework from the rhombic unit cell to an aggregate-bed scale by employing a simple and mechanistic up scaling scheme. This paper emphasizes static and steady external stress; extension to transient stresses such as imposed by passage of a tractor, will be presented in a subsequent work.

THEORY

We represent a soil aggregate bed as an assembly of discrete structural units. The structural units are embodied in mathematically tractable and simple geometric constructs that retain many of the features and structural behavior of a real soil. We calculate the deformation of unit elements under the influence of steady stress using rheological properties of the soil that forms the aggregates. Subsequently, the unit element model is up scaled to an aggregate bed model by considering stress and strain propagation in a one-dimensional stack of unit elements.

Basic Structural Unit Cell

The size, shape, and spatial arrangement of soil aggregates vary widely, and the processes of soil aggregate bed deformation nonlinearly depend on these factors. For mathematical tractability, we represent soil aggregates by spheres, and their spatial arrangements by simple packing geometries. The simplest packing systems often have the following features: (i) they are monodisperse, (ii) they are continuous, in that each sphere in the pack can be reached from any other sphere by crossing surface contacts only, and (iii) the density of the pack is uniform throughout the system. In cubic packing (Fig. 1a) each sphere is in contact with six other spheres (coordination number, $N = 6$) with internal porosity (ϕ) of 47.6%. Whereas in the rhombic packing (Fig. 1b) each sphere is in contact with 12 other spheres ($N = 12$) and has a porosity (ϕ) of 26.5%. For most aggregated soils the porosity of interest lies between these extremes. Two common approaches exist for building packing systems having intermediate porosity using the above unit cell configurations. In the first approach, a cubic unit cell made of eight spheres is transformed to a rhombohedral cell by sliding one of the layers, such that the displacements in the *x-y* plane are equal. The amount of movement is given by the angle, θ, measured between centers of spheres on the same side of the unit cell, and varies between 90° for cubic and 60° for rhombohedral (e.g., Kezdi, 1964). The formula for the porosity of the unit cell as a function of the packing angle θ is given as

$$\phi = 1 - \frac{\pi}{6(1 - \cos\theta)\sqrt{1 + 2\cos\theta}}. \qquad [1]$$

In the aforementioned transformation of a unit cell, the coordination number (N) does not vary continuously. In a second approach, the aggregate system is represented as a

T.A. Ghezzehei, Earth Science Division, Lawrence Berkeley National Laboratory, One Cycotron Road, MS90-1116, Berkeley, CA 94720; D. Or, Dep. of Civil and Environmental Engineering, University of Connecticut, 261 Glenbrook Road, Unit 2037, Storrs, CT 06269. Received 10 Oct. 2001. *Corresponding author (TAGhezzehei@lbl.gov).

Published in Soil Sci. Soc. Am. J. 67:12–19 (2003).

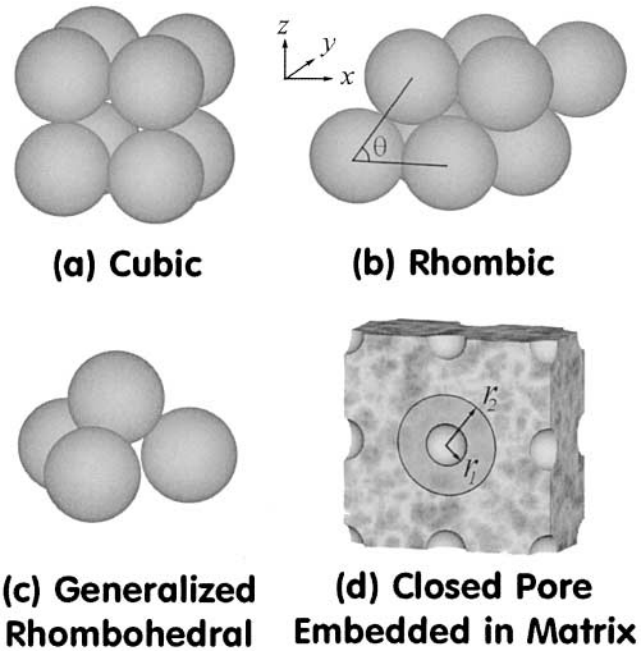

Fig. 1. Basic structural units. (a) Spheres in cubic packing, (b) spheres in rhombic packing, (c) generalized rhombohedral unit, and (d) spherical pore of radius r_1 embedded in homogeneous spherical matrix of radius r_2 ($r_1 - r_2$ is the thickness of the solid shell associated with the given pore).

composite made of clusters of cubic and rhombohedral arrangements, such that the proportion of the clusters yields the desired composite porosity. This approach leads to the following expression for the average coordination number, N, in terms of the porosity, ϕ (Smith et al., 1929):

$$N = 26.5 - 10.7/(1 - \phi). \quad [2]$$

In this study, we adopt a less-used third approach that employs a generalized rhombohedral unit (Fig. 1c) (Farouki and Winterkorn, 1964). The porosity of the rhombohedral unit ranges between that of cubic and rhombic packings. The rhombohedral unit was chosen because the formulae of contact forces are symmetric and can be computed with relative ease from simple geometric relationships.

In the rhombohedral unit, the gap formed between three monosized spheres (radius = a) supports a fourth sphere of same size as shown in Fig. 1c and 2. The volume of one unit cell is bound by a tetrahedron connecting the centers of the spheres as shown in Fig. 2a. The three bottom spheres need not be in contact with each other. The angle θ, is defined as the angle between the line connecting the upper sphere with a lower sphere and the plane of the three lower spheres, and its value ranges from 35° (equivalent to cubic packing) to 54° (equivalent to rhombic packing).

Consider a unit cell subjected to an average downward stress, Σ, which can be related to the external stress, as will be shown later. The force acts on the effective planar area of the unit cell, shown as a shaded region in Fig. 2a and 2b. In response to the applied stress, the center of the top sphere approaches the centers of the bottom spheres by 2ε, where ε is the contact strain (as shown in subsequent subsection). This also leads to an increase in the interaggregate contact area. The resulting vertical downward force, F_T, acting at the top of the cell, is given as a function of the planar area of the unit cell by

$$F_T - \Sigma A, \quad [3]$$

where $A = 3\sqrt{3}[a(1 - \varepsilon)\cos\theta]^2$ is the planar surface area of

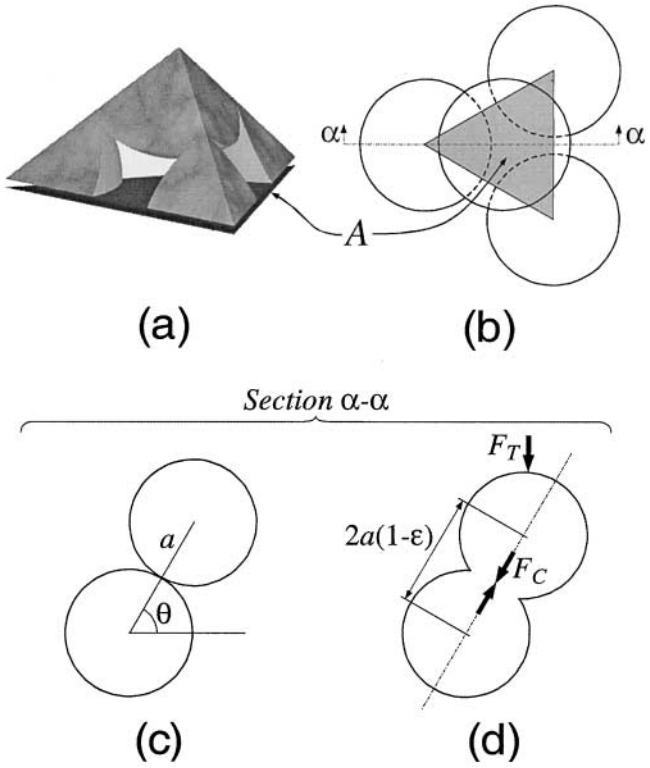

Fig. 2. Definition of variables for the generalized rhombohedral system. (a) Truncated unit cell, (b) planar area of the unit cell, (c) packing angle, and (d) strain.

the unit cell (shaded area in Fig. 2a and 2b). By symmetry, the total force Eq. [3] is equally divided among the three interaggregate contacts of the unit cell. The contact force (F_c) and contact stress (σ) at each of the three contacts are, respectively, given by

$$F_C = \frac{F_T}{3\sin\theta}, \quad [4]$$

$$\sigma = \frac{F_c}{2\pi a^2 \varepsilon} = Q\frac{(1 - \varepsilon)^2}{\varepsilon}, \quad [5]$$

where $Q = \sqrt{3}\,\Sigma\cos\theta/[2\pi\tan\theta]$ is collection of the constants in Eq. [3] and [4] and represents the stress applied at a contact modified by the packing angle. Its value is directly proportional to the external stress Σ, and inversely related to the packing angle θ. The term $2\pi a^2\varepsilon$ in Eq. [5] is an approximation of the interaggregate contact area (Scherer, 1984). The porosity of the unit cell, ϕ, is given as a function of the angle θ and strain ε by

$$\phi = 1 - \frac{\pi}{9\sqrt{3}\sin\theta\cos^2\theta}\frac{1}{(1 - \varepsilon)^2}. \quad [6]$$

We define a relative density of the unit cell as a ratio of the absolute cell density, ρ_c, to the absolute aggregate density, ρ_a,

$$\rho = \rho_c/\rho_a = 1 - \phi. \quad [7]$$

The mechanics of contact deformation under steady external stress is presented in next subsection.

Deformation of a Unit Cell

Soil deformation is considered to occur under steady-stress condition if the rate of change of stress is small compared with

Table 1. Viscoplastic Coefficients of Millville Silt Loam Soil at Different Water Contents.

Water Content	τ_y	η_p
kg kg^{-1}	Pa	Pa s
0.34	300	17 000
0.30	950 (1 900)†	50 000
0.28	1 225 (2 450)	60 000
0.25	4 000 (8 000)	180 000

† Values in parentheses were used in Fig. 7.

the strain rate. This assumption permits the implementation of soil rheological properties measured under steady shear stress.

Rheological Properties of Soil Under Steady Stress

The relationship between shearing stress, τ (Pa), and shearing rate, $d\gamma/dt(s^{-1})$, of wet soils can be described by the Bingham rheological model (Ghezzehei and Or, 2001; Vyalov, 1986):

$$\tau - \tau_y = \eta_p \, d\gamma/dt, \qquad [8]$$

where η_p (Pa s) is the coefficient of plastic viscosity, τ_y (Pa) is the yield stress, and γ is shear strain. Equation [8] is the simplest viscoplastic model, and states that viscous flow commences only when the applied stress τ exceeds the yield stress of the soil τ_y. Ghezzehei and Or (2001) determined the rheological coefficients (η_p and τ_y) of different soils and clays using a rotational rheometer. The rheometer applies a shearing stress, τ, to a wet soil sample contained between a pair of parallel discs (35 mm in diam.) and the resulting shear strain, γ, and strain rate, $d\gamma/dt$ are determined. For subsequent illustrative examples, we use the rheological properties of Millville silt loam soil (Coarse-silty, carbonatic, mesic Typic Haploxerolls) at four different water contents given in Table 1.

Deformation of a Unit Cell under Steady Stress

Consider a constant stress, Σ, acting at the top of the unit cell, and a contact stress between two aggregates, σ, as defined by Eq. [5]. Assuming that the soil aggregates obey the Bingham law in compression, the general equation governing the coalescence process is given as (Vyalov, 1986)

$$\frac{d\varepsilon}{dt} = \frac{\sigma - \sigma_y}{\lambda_p}, \quad \sigma > \sigma_y,$$
$$\frac{d\varepsilon}{dt} = 0, \quad \sigma \le \sigma_y, \qquad [9]$$

where $\lambda_p = 3\eta_p$ is the coefficient of plastic viscosity in compression and $\sigma_y = \tau_y/2$ is the yield stress in compression (Vyalov, 1986). These transformations of coefficients from shear to compression are based on the assumption that the soil forming the aggregates is incompressible. The strain under steady stress is obtained by solving Eq. [9], subject to the initial condition $\varepsilon(t = 0) = \varepsilon_o$, and is implicitly given as:

$$\frac{2(2 + 1/L)}{\sqrt{-4/L - 1/L^2}}\left\{\arctan\left[\frac{2(\varepsilon - 1) - 1/L}{\sqrt{-4/L - 1/L^2}}\right] - \arctan\left[\frac{2(\varepsilon_o - 1) - 1/L}{\sqrt{-4/L - 1/L^2}}\right]\right\}$$
$$+\ln\left[\frac{(\varepsilon - 1)^2 - \varepsilon/L}{(\varepsilon_o - 1)^2 - \varepsilon_o/L}\right] = 2\frac{Q}{\lambda_p} \cdot t \qquad [10]$$

where the load ratio $L = Q/\sigma$ describes the magnitude of the applied stress relative to the rheological yield stress of the soil. In Fig. 3 the strain, ε, is plotted as a function of nondimensional time tQ/λ_p for several values of the load ratio L.

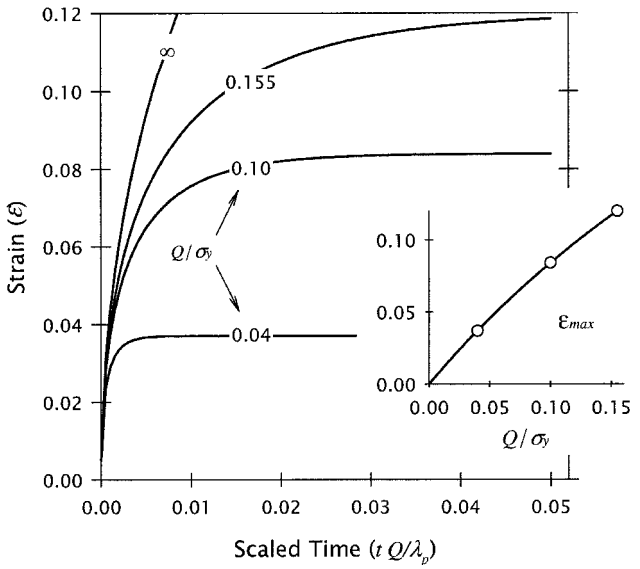

Fig. 3. Viscoplastic strain of a generalized rhombohedral system as a function of nondimensional time for various dimensionless load ratios. Inset: The maximum strain as a function of the dimensionless load ratio (circles denote the load-ratio values used in the main plot).

The general feature of the solutions shown in Fig. 3 is that strain increases with nondimensional time at a decreasing rate until it reaches a maximum value. The decreasing rate of deformation is because of inverse relationships between strain, ε, and contact stress, σ, in Eq. [5]. Moreover, at any given nondimensional time, a higher load ratio, L, results in a higher strain, ε. The magnitude of the load ratio depends on three quantities: the applied external stress (Σ), rheological yield stress (τ_y), and the packing angle of the unit cell (θ). Increasing the external stress (Σ) or decreasing the yield stress (τ_y) results in a higher load ratio (L). From Fig. 2 and Eq. [5], we recall that loose packings have low packing angle (θ) and result in higher applied stress (Q). This implies that loose packs are more prone to deformation than denser packs with a stiffer structure. The nondimensional time Qt/λ_p indicates that the time required to attain a given strain value is inversely proportional to the applied stress, Q, and directly proportional to the viscosity, λ_p. The maximum strain, ε_{max}, that can be achieved with a given load ratio, L is determined by solving Eq. [9] when deformation ceases, that is $d\varepsilon/dt = 0$:

$$\varepsilon_{max} = 1 + \frac{1}{2L} - \sqrt{\frac{1}{L} + \frac{1}{4}\frac{1}{L^2}}. \qquad [11]$$

This equation is plotted as an inset in Fig 3. Equation [11] asserts that the ultimate strain depends only on the load ratio L, and not on the viscosity or initial strain state.

Deformation under Constant Strain Rate

Under certain experimental conditions a soil sample may be subjected to constant strain rate ($\dot{\varepsilon}$) while recording stress and strain continuously (e.g., Braunack and Dexter, 1978). For such experiments, the stress–strain relationship pertaining to a unit cell is obtained by setting the strain rate in Eq. [9] (left-hand side) to a constant, that is $d\varepsilon/dt = \dot{\varepsilon}_c$:

$$\varepsilon = 1 + \varepsilon_o + \frac{1}{2}\left(\frac{1}{L} + \frac{\lambda_p}{Q}\dot{\varepsilon}_c\right) - \left\{\left(\frac{1}{L} + \frac{\lambda_p}{Q}\dot{\varepsilon}_c\right)\right.$$

$$+ \frac{1}{4}\left(\frac{1}{L} + \frac{\lambda_p}{Q}\dot{\varepsilon}_c\right)^2\Bigg\}^{1/2}. \quad [12]$$

The time corresponding to a given strain (ε) could be obtained from the constant strain rate $d\varepsilon/dt = \dot{\varepsilon}_c$ as

$$t = \frac{\varepsilon - \varepsilon_o}{\dot{\varepsilon}_c}. \quad [13]$$

Transition from Coalescence of Discrete Aggregates to Shrinkage of Closed Pores

It is important to note that the above discrete representation of the soil aggregates applies to the loose state of soil aggregate bed, while adjacent interaggregate contacts are not overlapping and soil flow at the interaggregate contacts maintains radial symmetry. Beyond a certain cut-off strain value (ε_c), adjacent contact regions begin to overlap and modify the radial flow pattern of soil material. Subsequent deformation involves restricted and complex flow pathways, which continues until adjacent pores are isolated. For the later stages of deformation involving shrinkage of pores, we use an adaptation of a model developed by Mackenzie and Shuttleworth (1949) that considers shrinkage of spherical pores embedded in a uniform Newtonian-viscous or Bingham-viscoplastic matrix. We present the details of this approach in a separate article (Ghezzehei and Or, 2003). The transition zone from coalescence of discrete aggregates to shrinkage of isolated pores remains unexplained by either of the two approaches (Scherer, 1979; Scherer, 1984).

For the loosest aggregate packing ($\theta = 35°$), the maximum strain (ε_c) that can be explained by coalescence of aggregates is approximately $\varepsilon_c = 0.12$ (Ghezzehei and Or, 2000). Although the value of this critical strain (ε_c) decreases slightly with packing angle, for simplicity, we apply $\varepsilon_c = 0.12$ as a constant cut-off strain for all packing angles.

Shrinkage of Closed Pores under Steady Stress

For completeness, only the end results of Ghezzehei and Or (2003) used in subsequent illustrative examples are repeated in this subsection. The model of Mackenzie and Shuttleworth (1949) considers a spherical pore of radius r_1 surrounded by a concentric solid shell of radius r_2 as shown in Fig. 1d. The density of the pore-shell system relative to the shell density is defined as

$$\rho = \frac{\text{density of pore + shell}}{\text{density of shell}} = 1 - (r_1/r_2)^3. \quad [14]$$

Considering a soil matrix obeying Bingham-viscoplastic flow behavior, Eq. [8], the maximum density that can be achieved under steady stress is given by

$$\rho_{max} = 1 - \exp\left(-\frac{\sqrt{2}}{2}\cdot\frac{\Sigma_{oct}}{\tau_y}\right), \quad [15]$$

where $\Sigma_{oct} = (\Sigma_1 + \Sigma_2 + \Sigma_3)$ is the octahedral stress, defined as a mean of the stresses acting in the principal axes. Note that Eq. [15] is equivalent to Eq. [11], in the sense that they both represent the maximum density (strain) after sufficiently long period and are dependent only on stress ratios but not on viscosity or time. Equation [15] depends only on the ratio of the octahedral stress to yield stress (Σ_{oct}/τ_y) similarly Eq. [11] depends only on the load ratio L.

Under constant strain rate ($d\varepsilon/dt = \dot{\varepsilon}_c$), the relationship between the relative density and the external stress is given by

$$\frac{\rho^2}{\rho_o}\dot{\varepsilon}_c = \frac{3}{4}\cdot\frac{\Sigma_{oct}}{\eta_p}(\rho - 1)\left\{1 + \frac{\sqrt{2}\cdot\tau_y}{\Sigma_{oct}}\ln[1-\rho]\right\}. \quad [16]$$

where ρ_o is the initial density at $\varepsilon = \varepsilon_o$. Note that Eq. [16], as Eq. [12], applies to experimental conditions in which a soil sample is subjected to constant strain rate.

An Aggregate Bed

Up scaling of individual unit cell dynamics to a sample scale requires consideration of: (i) spatial arrangement of unit cells, and (ii) interaction between unit cells. As shown in the previous sections, the stress-strain relations are nonlinear even at the scale of a unit cell. To perform the up scaling in a mathematically tractable way, without resorting to homogenization and continuum approaches, it is necessary to use simplified spatial structure of unit cells and employ a sufficiently simple description of force and stress transmission between adjacent unit cells.

Spatial Arrangement of Unit Cells

We represent a bed of soil aggregates by a vertical, one-dimensional stack of unit cells. Each unit cell represents a monolayer of aggregates, as shown in Fig. 4a and 4b. In principle, the physical properties of the unit cells in any given layer (e.g., aggregate size, packing angle, initial strain, or rheology) need not be identical, so long as an effective unit cell can represent them. The different layers in the profile could differ in physical properties. In this study, we limit the orientation

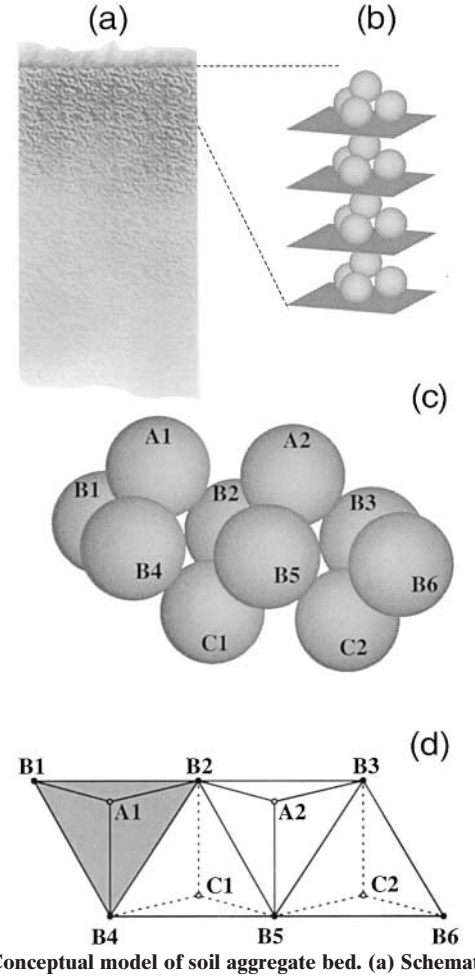

Fig. 4. Conceptual model of soil aggregate bed. (a) Schematic representation of soil aggregate bed, (b) one-dimensional array of unit cells separated by conceptual rigid planes (c) one layer of close-fitting unit cells, (d) planar view of a layer of unit cells.

of the unit cells such that the widest surface of the tetrahedral unit cell is parallel to the horizontal plane. Additional variability could be introduced to the problem by considering a statistical distribution of orientation angle of the unit cells. However, this would result in nonuniform stresses and strains in the three contacts of the unit cell, and involves more complicated geometrical relationships than presented here.

Stress Propagation

The external stress, Σ, loosely defined in the preceding subsections is redefined here with rigor. In Fig. 4c, a portion of a layer comprising four closely matching unit cells is shown. The plane view of these cells, shown in Fig. 4d, suggests that the area occupied by an individual unit cell is equal to the triangular area, A, defined previously in Fig. 2. Therefore, the stress acting on a unit cell, Σ, is also identical to the stress acting on the entire layer of unit cells. For the topmost (surface) layer, this Σ is equal to the surface stresses.

Accounting for exact stress transmission requires consideration of all the geometric details regarding the contacts between aggregates. To retain the analytical capability of the present model, we employ a simple area-averaging approach for stress transmission. We introduce a conceptual rigid plane that carries the external load and uniformly distributes the stress to the top layer (unit cell). Similar conceptual stress-homogenization planes separate each layer as shown in Fig. 4b. This amounts to summing up the weight carried by a layer and transmitting it uniformly to the layer below. This consideration, while providing the required mathematical simplicity, imposes two limitations. First, it does not permit spatial localization of stresses and strains that has been demonstrated by numerical simulation and experiments using packs of granular materials (Calvetti and Emeriault, 1999; Radjai et al., 1998; Thornton and Antony, 1998). Second, because the stresses are mediated through horizontal planes, lateral components of stress transmission and dissipation are not accounted for.

Stress transmission is a time dependent process as governed by soil rheology. When subjected to steady external stress, a soil aggregate bed exhibits a Bingham viscoplastic behavior. The soil material at every interaggregate contact deforms whenever the applied stress exceeds the yield stress of the soil. During deformation, because the soil is considered to be under viscous condition, the stress is absorbed (dissipated) at the contact. As deformation progresses, the interaggregate contact grows, and the contact stress diminishes. When the contact stress falls below the yield stress, deformation ceases and the entire quantity of the stress is transmitted to the subsequent layer. The stress transmission condition can be expressed mathematically as

$$(\tau)_i > (\tau_y)_i \rightarrow \Sigma_{i+1} = 0$$
$$(\tau)_i \leq (\tau_y)_i \rightarrow \Sigma_{i+1} = \Sigma_i \qquad [17]$$

where i denotes the number of layers with $i = 1$ being the top layer. Then, the strain at the i_{th} layer is calculated using Σ_i in Eq. [10].

Illustrative Examples

The analytical framework presented above is general and can be used to study several scenarios of practical and theoretical interest. As it would be difficult to exhaust all the possible combinations of conditions, we restrict the illustrative examples to a few scenarios that represent the most important features of the proposed models. Whenever possible, we compare the theoretical results with experimental results from the literature. Some of the comparisons are only qualitative, as all the required information pertaining to the experimental data (mainly rheological properties) are unknown. We present three different examples of soil aggregate bed deformation under steady stress; each highlights specific features of the models presented in this study.

Isotropic Compression of Synthetic Aggregates

In this example, we examine the ultimate strain Eq. [11] and maximal density Eq. [15] that results at a given external stress. The model performance is tested by comparison with isotropic compression of packs of spheres made of oil-based modeling clay, reported by Davis et al. (1973). Spheres approximately 8 mm in diameter were made from modeling clay of plastic consistency. The spheres were arranged in cubic and rhombic packings inside a cylindrical rubber membrane of 100-mm diam. and 100-mm height. The samples were isotropically compressed inside a standard triaxial cell. The volume decrease of the sample in response to applied stress was determined by monitoring the volume of air (under constant pressure) leaving the sample. Davis et al. (1973) scaled the stress by the yield stress of the modeling clay, determined using frictionless indentation by a sphere. For the subsequent comparisons, we considered the yield stress of the modeling clay determined by the indentation experiments as equivalent to the yield stress in compression, σ_y. Hence, the nondimensional stress reported by Davis et al. (1973) is equivalent to our Σ/σ_y in Eq. [11].

In Fig 5a, the maximum strain Eq. [11] is plotted as a function of nondimensional load (Σ/σ_y) for the two packing modes. Although Davis et al. (1973) indicated that they had cubic and rhombic packings, the initial densities suggest that the packings were imperfect. Thus, the packing angles for our calculations were determined from the initial density (porosity) using Eq. [6]. The resulting packing angles for the cubic and rhombic systems were $\theta = 38°$ and $\theta = 51.5°$, respectively (compare with $\theta = 35.3°$ and $\theta = 54.7°$ for ideal cubic and rhombic packings, respectively). The calculated and measured relative densities, plotted in Fig 5b, show reasonable agreement up to the critical strain $\varepsilon = 0.12$.

For deformation beyond the critical strain, the model of radial shrinkage of isolated pores, Eq. [15], was used. The shrinkage of closed pores does not depend on the original packing geometry; hence the same model prediction applies to both packing angles. The maximum density of the samples ($\rho = 0.95$) at the highest stresses was less than the ideal maximum density of $\rho = 0.95$, which could be attributed to air pressure built up as the pores get completely isolated. Therefore, good agreement between the measured and predicted densities was obtained by introducing ultimate density of $\rho = 0.95$ to the original model Eq. [15] which did not consider such limitations,

$$\rho_{max} = 0.95 - \exp\left(-\frac{\sqrt{2}}{2} \times \frac{\Sigma_{oct}}{\tau_y}\right). \qquad [18]$$

After attainment of the critical strain $\varepsilon_c = 0.12$, the evolution of the pore geometry toward spherical shape is gradual. Consequently, during the transition from the coalescence of distinct spheres to radial shrinkage of spherical pores, neither of the two models describes the process adequately, as shown in Fig. 5b.

Uniaxial Compression of Soil Aggregate Bed

The above example is somewhat limited in the sense that it was concerned with the maximum density only with no time dependent information. In this second example, we emphasize

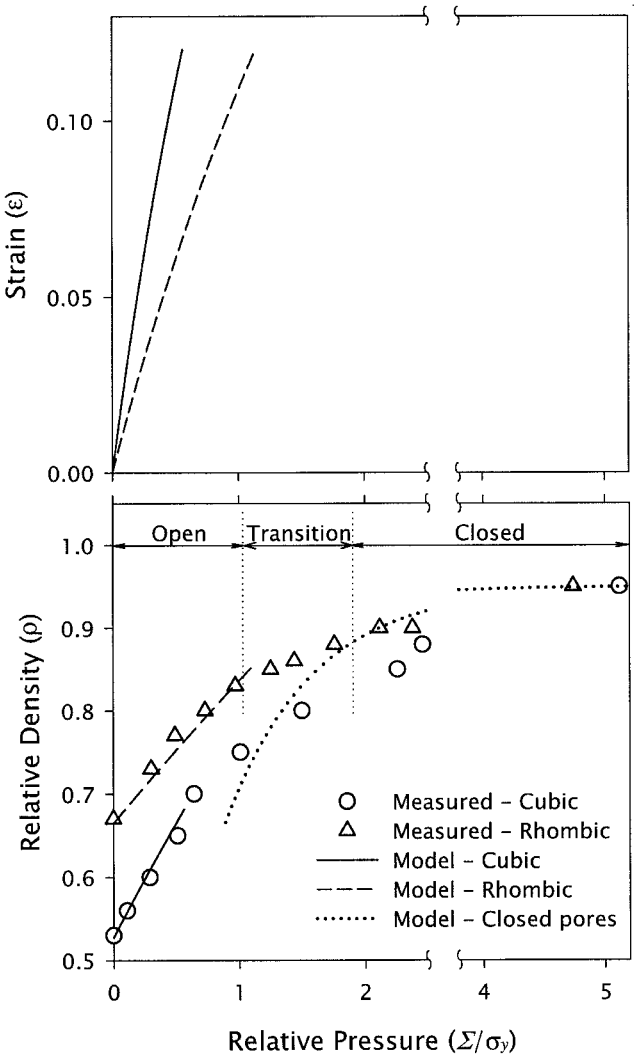

Fig. 5. Coalescence of modeling clay under isotropic stress. (a) Strain as a function of dimensionless stress. (b) Relative density as a function of dimensionless stress, for two packing angles. Note that for closed pores the original packing is irrelevant.

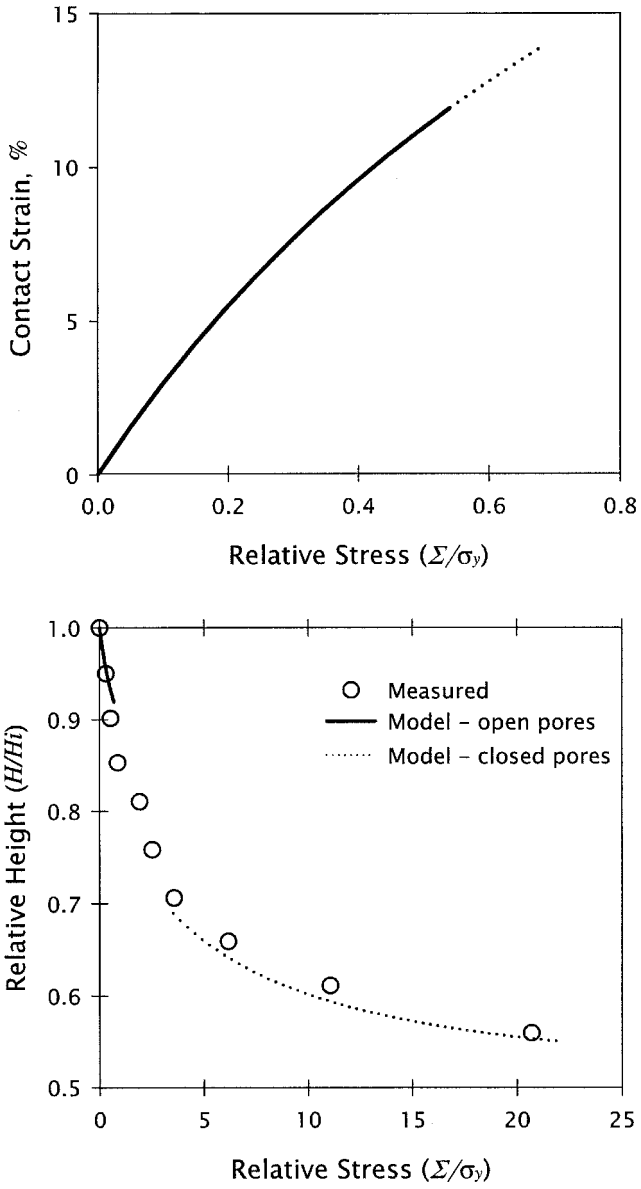

Fig. 6. Coalescence of natural soil aggregates under uniaxial stress, at constant strain rate. (a) Strain as a function of dimensionless stress. (b) Relative density as a function of dimensionless stress.

the time-dependence of soil deformation. For comparison, we use uniaxial compression data of natural soil aggregate bed reported by Braunack and Dexter (1978). Different sizes of aggregates of Urrbrae loam soil (Australia) were collected by sieving. The ratio of the major/intermediate/minor axes of the aggregates was 1.0:0.8:0.6 for all the size classes. The aggregates were wetted to saturation by capillary action and then dried to required matric potential using a pressure-plate apparatus. The wetted aggregates were packed in cylindrical compression cells of 80-mm diam. and 100-mm height, and compressed uniaxially at a strain rate of 0.021 mm s^{-1} ($\dot{\varepsilon} = 2.1 \times 10^{-4}$ s^{-1}). The height of the samples H was recorded as a function of the axial stress P. The stress P was scaled by the tensile yield strength of the individual aggregates Y, measured by the force F required to crush them between parallel plates. The yield strength Y was determined by an empirical relationship,

$$Y = 0.576F/d^2. \quad [19]$$

where d is the mean aggregate diameter. The dataset used for this illustrative example was that of 5.1 to 9.5 mm diam. aggregates at water content of 0.3 kg kg^{-1} and matric potential of −10 kPa (Braunack and Dexter, 1978). The tensile yield strength determined by the procedure described above was 21 kPa.

In Fig. 6a, the strain, ε, because of coalescence of spherical aggregates is plotted as a function of the scaled axial stress, Σ/σ_y, using Eq. [12], and the results are replotted in terms of relative sample height ($1 - \varepsilon$) in Fig. 6b. Note that we are assuming equivalence between Σ/σ_y of our model and P/Y of Braunack and Dexter (1978). In view of the large deformations observed in the experimental data, we modeled the aggregate bed using the loosest possible packing angle of $\theta = 35°$. Although the range of deformation that was modeled by coalescence of distinct aggregates was small, a good match between predicted and measured values was obtained. The compression beyond the critical strain $\varepsilon_c = 0.12$ was described by the model of radial shrinkage of spherical pores Eq. [16]. The calculated pack density was translated to relative sample height by the relationship,

$$H/H_i = \frac{\rho_o}{\rho}. \quad [20]$$

Because the actual viscosity of soil aggregates was not known, the ratio Σ/η_p was used as a fitting parameter in the above calculations. The value of the ratio that resulted in the best agreement was $\Sigma/\eta_p = 500$ (viscosity of $\eta_p = 200$ kPa). These comparisons are intended to demonstrate the plausibility of the proposed model. Further experimental work is required for quantitative comparison and model testing.

Soil Aggregate Bed Compression by Overburden

Most agricultural soils are not subjected to external steady load. However, wetting of a dry soil-aggregate bed could reduce the soil yield stress to below the overburden stress (exerted by the weight of the overlying soil), thereby initiating a steady-state deformation. In this example, we present deformation of an aggregate bed as the water content is raised from air-dry to three successively wetter stages. In nature, soil wetting is a spatially and temporally variable process and nonlinearly depends on the consequences of the soil aggregate bed deformation (see Or et al., 2000 for details). As a result, the deformation depends on the coupling of the flow and deformation processes. The maximum strain and density, however, are functions of only the stress distribution in the aggregate bed and the yield stress of the soil at the specific water content. This example focuses on the maximum density profile of an aggregate bed.

For qualitative evaluation of the model calculations, we present experimental data of strain profile in Millville silt loam soil columns reported by Ghavami et al. (1974). Millville silt loam soil passing through a 2-mm sieve was lightly compacted in a cylinder (600 mm in length and 150 mm in diam.) to an initial bulk density of 1200 kg m^{-3}. Water was applied to the top of the column at rates of 6.35, 12.70, and 25.4 mm h^{-1} by a rotating water applicator. The matric potential of the soil column was regularly monitored using tensiometers installed at a 76-mm interval. The average matric potential and water content in the soil column varied with the water application rate. The matric potential was held constant for each application rate by applying suction to a porous ceramic plate placed at the bottom of the column. Soil settlement was regularly monitored at 38-mm thick layers (16 layers) separated by markers. The strains of the 38-mm thick layers under 76, 152, 305, and 533 mm overburden and at different water contents are plotted in Fig. 7.

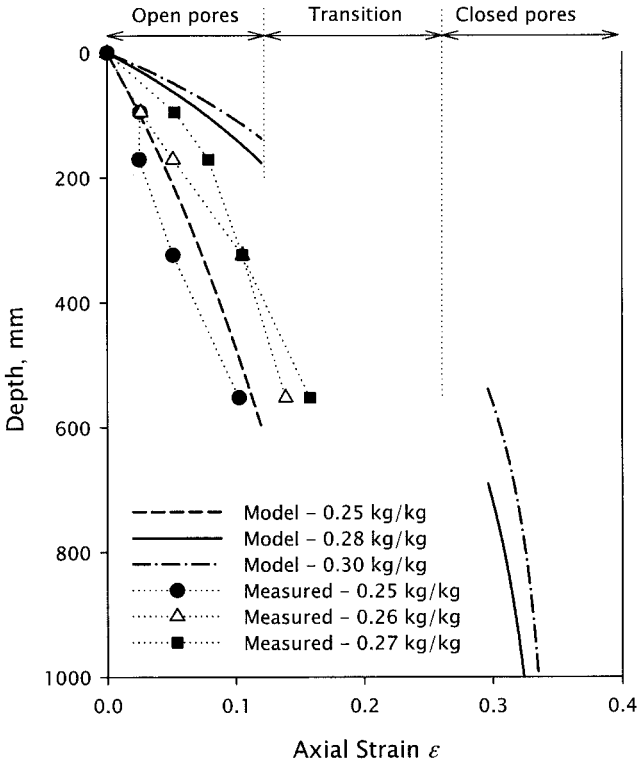

Fig. 7. Strain profile in Millville silt loam soil. Measured values correspond to soil columns of soil passing through 2-mm sieve (Ghavami et al., 1974). Model values correspond to calculations using an aggregate bed made of 2-mm aggregates.

In this example, we represent the settlement process by considering a hypothetical aggregate bed constructed of aggregates of 2-mm diam. We consider that the aggregates are arranged in the densest unit cell packing angle of $\theta = 54°$ to account for the dense packing that naturally occurs in packs of different sizes (note that the experiment was conducted using aggregates <2-mm in diam.). The density of individual aggregates was set to 1650 kg m^{-3} to obtain an unit cell density of 1200 kg m^{-3}, comparable with the experiments. The resulting height of the unit cell was 0.77 mm, and a total of 620 layers (equivalent to aggregate-bed depth of 1 m) were considered in the calculations. Each layer was subjected to the wet weight of the aggregates above it, and the corresponding contact stress was calculated using Eq. [5]. The coalescence of the aggregates when the strain was less than the critical strain of $\varepsilon_c = 0.12$ was calculated using Eq. [11], and the densification beyond that critical strain was determined using Eq. [15]. These calculations were performed at 0.25, 0.28, and 0.30 kg kg^{-1} water content, for which Ghezzehei and Or (2001) reported the corresponding rheological properties. The calculated axial strains are plotted as a function of depth in Fig. 7. As the total soil fraction <2 mm was modeled as a monodisperse aggregate bed (2-mm aggregates), the model unit cells are likely to have a softer geometrical structure because of fewer interaggregate contacts. For illustrative purposes, we accounted for this discrepancy by doubling the yield stress in the model calculations (see Table 1).

The increase in water content has a dual effect; it increases the overburden while decreasing yield strength (and soil viscosity). This combined effect of a uniformly higher water content results in more densification to larger depths. The trends of the model calculations and experimental results are comparable. Model calculations at 0.25 kg kg^{-1} water content match experimental measurements at the same water content. The experimental results at 0.26 and 0.27 kg kg^{-1} are bound by model calculations at higher water contents of 0.28 and 0.30 kg kg^{-1}. The model does not consider the extreme case where the entire soil pore space is fully saturated; consolidation under saturated conditions are described by the well-established Terzaghi's theory (Mitchell, 1993).

SUMMARY AND CONCLUSIONS

We presented new models for describing densification of uniform soil aggregate bed under steady external stress, using mathematically tractable geometry. Soil aggregates were represented by a unit cell made of equal-sized spherical aggregates, packed in a generalized rhombohedral arrangement. The rhombohedral packing provided a wide range of initial porosity and stiffness, and symmetrical distribution of stresses within the unit cell. Interaggregate stresses and strains and associated changes in density and porosity were calculated for each unit cell using rheological properties of the soil that forms the aggregates.

The modeling approach proposed in this study couples the two main components that determine structural dynamics of aggregated soil: (i) the geometry and spatial arrangement of soil aggregates, and (ii) the intrinsic properties (i.e., rheology) of the aggregate forming soil. A significant advantage of this approach over the traditional soil mechanics is that the rheological properties of soil can be characterized independently of the soil aggregation and strain state. Moreover, by focusing on pore-scale dynamics, this study provides a link between mechanical transformation of soil structure and evolution of soil hydraulic properties. Despite the simplicity of the geometrical models used to represent aggregates and their spatial arrangement, the models capture the major trends of soil compression under steady stress, as demonstrated by the illustrative examples. More detailed experimental work is required to quantitatively validate and improve the models presented in this study.

APPENDIX

Notation

a = Aggregate radius, m
A = Planar surface area of unit cell, m^2
F_C = Contact force, N
F_T = Total force, N
L = Load ratio
N = Coordination number
Q = Constant
r_1 = Pore radius, m
r_2 = Shell radius, m
Σ = Average downward stress, N
$\Sigma_1, \Sigma_2, \Sigma_3$ = Principal mean stresses, N
Σ_{oct} = Octahedral stress, N
ε = Strain
ε_c = Maximum strain rate that can be explained by coalescence of discrete aggregates
ε_{max} = Maximum strain for load ratio of L.
ε_o = Initial strain
$\dot{\varepsilon}$ = Constant strain rate, s^{-1}
ϕ = Porosity
γ = Shear strain
η_p = Coefficient of plastic viscosity in shear, Pa s
λ_p = Coefficient of plastic viscosity in compression, Pa s
θ = Packing angle
ρ = Relative density, kg m^{-3}
ρ_a = Absolute aggregate density, kg m^{-3}
ρ_c = Absolute cell density, kg m^{-3}
ρ_{max} = Maximum density, kg m^{-3}
ρ_o = Initial density, kg m^{-3}
σ_y = Yield stress in compression, N
τ = Shear stress, N
τ_y = Yield stress in shear, N

Notations adopted from (Braunack and Dexter, 1978)

d = aggregate diameter, m
F = Crushing force, N
H = Sample height, m
H_i = Initial sample height, m
P = Axial stress, Pa
Y = Yield strength, Pa

ACKNOWLEDGMENTS

The partial funding by USDA/NRI through contract No. 9700814 and the US-Israel Binational Agricultural and Research Fund (BARD) through contract No. 2794-96 are gratefully acknowledged. The work reported herein was performed at Plants, Soils, and Biometeorology Department, Utah State University, Logan, UT.

REFERENCES

Braunack, M.C., and A.R. Dexter. 1978. Compaction of aggregate beds. p. 119–26. *In* W.W. Emerson et al. (ed.) Modification of Soil Structure. John Wiley & Sons, New York.

Calvetti, F., and F. Emeriault. 1999. Interparticle forces distribution in granular materials: Link with the macroscopic behaviour. Mech. Cohesive-Frict. Mater. 4:247–279.

Davis, P.F., A.R. Dexter, and D.W. Tanner. 1973. Isotropic compression of hypothetical and synthetic tilths. J. Terramech. 10:21–34.

Ghavami, M., J. Keller, and I.S. Dunn. 1974. Predicting soil density following irrigation. Trans. ASAE 17:166–171.

Ghezzehei, T.A., and D. Or. 2003. Stress-induced Shrinkage of isolated pores. Water Resour. Res. (in press).

Ghezzehei, T.A., and D. Or. 2001. Rheological properties of wet soils and clays under steady and oscillatory stresses. Soil Sci. Soc. Am. J. 65:624–637.

Ghezzehei, T.A., and D. Or. 2000. Dynamics of soil aggregate coalescence governed by capillary and rheological processes. Water Resour. Res. 36:367–379.

Horn, R., B.G. Richards, W. Grasle, T. Baumgartl, and C. Wiermann. 1998. Theoretical principles for modelling soil strength and wheeling effects—A review. Z. Pflanzen. Bodenk. 161:333–346.

Kezdi, A. 1964. Discussion on "Mechanical properties of granular systems" by N. A. Farouki, and H. F. Winterkorn. Highway Res. Rec. 52:42–58.

Kirby, J.M. 1994. Simulating soil deformation using a critical-state model: I. Laboratory tests. Eur. J. Soil Sci. 45:239–248.

Kirby, J.M., B.G. Blunden, and C.R. Trein. 1997. Simulating soil deformation using a critical-state model: II Soil compaction beneath tyres and tracks. Eur. J. Soil Sci. 48:59–70.

Koolen, A.J., and H. Kuipers. 1989. Soil deformation under compressive forces. p. 32–52. *In* W.E. Larson et al. (ed.) Mechanics and Related Processes in Structured Agricultural Soils. Kluwer Academic Publishers, Dordrecht.

Lebert, M., N. Burger, and R. Horn. 1989. Effects of dynamic and constant loading on compaction of structured soils. p. 73–82. *In* W.E. Larson et al. (ed.) Mechanics and Related Processes in Structured Agricultural Soils. Kluwer Academic Publishers, Dordrecht.

Mackenzie, J.K., and R. Shuttleworth. 1949. A phenomenological theory of sintering. Proc. Phys. Soc. 62:833–852.

Mitchell, J.K. 1993. Fundamentals of soil behavior. 2nd ed. John Wiley and Sons, New York.

Oda. M., and K. Iwashita (ed.) 1999. Mechanics of granular materials. A.A. Balkema, Rotterdam.

Or, D. 1996. Wetting induced soil structural changes: The theory of liquid phase sintering. Water Resour. Res. 32:3041–3049.

Or, D., F.J. Leij, V. Snyder, and T.A. Ghezzehei. 2000. Stochastic model for post-tillage soil pore space evolution. Water Resour. Res. 36:1641–1652.

Radjai, F., D.E. Wolf, M. Jean, and J.J. Moreau. 1998. Bimodal character of stress transmission in granular packings. Phys. Rev. Lett. 80:61–64.

Scherer, G.W. 1984. Viscous sintering of a bimodal pore-size distribution. J. Am. Ceram. Soc. 67:709–715.

Scherer, G.W. 1979. Sintering of inhomgeneous glasses: Application to optical wave guides. J. Non-Cryst. Solids 34:239–256.

Smith, W.O., P.D. Foote, and P.F. Busang. 1929. Packing of homogeneous spheres. Phys. Rev. 34:1271–1274.

Thornton, C., and S.J. Antony. 1998. Quasi-static deformation of particulate media. Philos. Trans. R. Soc. Lond. Ser. A 356:2763–2782.

Vyalov, S.S. 1986. Rheological Fundamentals of Soil Mechanics. Elsevier, New York.